Journal of Molecular Catalysis A: Chemical 335 (2011) 199–204

Contents lists available at ScienceDirect

Journal of Molecular Catalysis A: Chemical

journal homepage: www.elsevier.com/locate/molcata

Electro-oxidation of hydrazine on gold nanoparticles supported on TiO_2 nanotube matrix as a new high active electrode

Mirghasem Hosseini*, Mohamad Mohsen Momeni, Masoud Faraji

Electrochemistry Research Laboratory, Department of Physical Chemistry, Chemistry Faculty, University of Tabriz, Tabriz, Iran

ARTICLE INFO

Article history:
Received 14 July 2010
Received in revised form
10 November 2010
Accepted 27 November 2010
Available online 17 December 2010

Keywords:
Hydrazine electro-oxidation
Titanium dioxide nanotubes
Gold nanoparticle

ABSTRACT

Au/titanium dioxide nanotubes (Au/TiO_2-NTs) catalysts are prepared by a simple method using galvanic deposition of gold nanoparticles on TiO_2-NTs as support. TiO_2-NTs are fabricated by anodizing titanium foil in a dimethyl sulfoxide (DMSO) fluoride-containing electrolyte. Scanning electron microscope and energy-dispersive X-ray spectroscopy results indicate that nanotubular TiO_2 layers consist of individual tubes of about 50–80 nm diameters and gold nanoparticles with a size range of 30–40 nm are well-dispersed on the surface of TiO_2-NTs support. The electro-catalytic properties of Au/TiO_2-NTs catalysts toward electro-catalytic oxidation of hydrazine are investigated by cyclic voltammetry. Compared to flat gold electrodes, Au/TiO_2-NTs catalyst shows much higher electrochemical activity. This may be attributed to the uniform dispersion of gold nanoparticles on TiO_2-NTs, smaller particle size and unique properties of TiO_2-NTs support. In addition, the mechanism of hydrazine electrochemical oxidation catalyzed by Au/TiO_2-NTs is investigated.

1. Introduction

Direct methanol fuel cell is expected as a hopeful candidate for direct fuel cell application systems. However, the efficiency and power output of direct methanol fuel cells are low because of severe poisoning of the anode catalyst by reaction intermediates such as CO and methanol crossover through the electrolyte membrane [1]. Hydrazine is an important high-performance fuel in aerospace propulsion applications, which also impresses promising potential applications in fuel cells. Hydrazine is an ideal fuel for a direct fuel cell system because it does not exhaust environmentally loading materials such as CO_2. Hydrazine is a compound with high hydrogen content (12.5 wt.%). Its hydrogen storage capability is higher than that of sodium borohydride (10.6 wt.%) and equivalent to that of methanol. The direct hydrazine fuel cell demonstrates a higher electromotive force of 1.61 V which is close to that of the direct borohydride fuel cell (1.64 V) and higher than that of the direct methanol fuel cell (1.21 V). When hydrazine is used as a fuel to power the direct hydrazine fuel cell, only nitrogen and water will be formed. However, specific precautions should be observed when using hydrazine solution as a fuel for the direct hydrazine fuel cell because hydrazine is toxic and carcinogenic compound [2]. The direct hydrazine fuel cell concept was first suggested in the 1960s [3]. Very few researches on the direct hydrazine fuel cell development have been done [4–7]. It is considered that more attentions should be paid to develop the direct hydrazine fuel cell technology due to the merits mentioned above. Noble metals such as platinum [3], palladium [8,9], silver [10] and gold [11,12] are very active in the anodic oxidation of hydrazine. However, they tend to lose reactivity as they precipitate, aggregate or form a surface film. Immobilization of the noble metal nanoparticles in an active matrix may enhance the overall reactivity of the catalytic metal centers. The performance of electrodes mainly depends on the morphology properties and surface area of the electrodes. In order to retain its high electroactivity, different matrices have been used for the immobilization of noble metal particles. Among these, inorganic nanostructure materials are more promising because of their regular structure, high active surface area for immobilization of metal particles, and good chemical as well as thermal stability [13]. Since the discovery of carbon nanotubes, increasing attention has been paid to the study of nanostructures such as nanotubes, nanorods and nanowires. Titanium dioxide can be formed with different morphologies such as nanoparticles, nanofibres, nanotubes and nanosheets. Titanium dioxide nanotubes are very biocompatible, inexpensive, environmentally benign, and chemically as well as thermally stable inorganic material [14]. Titanium dioxide nanotube arrays have demonstrated a number of important applications including gas sensors, solar cells, photo-catalysts, tissue engineering, biosensors and electro-catalyst [15–18]. Our recent studies have shown that the immobilization of the metal nanoparticles in an active matrix improves the electro-catalytic activity to a great extent [19–24]. In the present work, we prepared a promising hydrazine electro-

* Corresponding author. Tel.: +98 4113393138; fax: +98 4113340191.
E-mail address: mg-hosseini@tabrizu.ac.ir (M. Hosseini).

1381-1169/$ – see front matter © 2010 Elsevier B.V. All rights reserved.
doi:10.1016/j.molcata.2010.11.034

catalyst based on the co-immobilization of gold nanoparticle on titanium dioxide nanotubes arrays and compared it with flat gold electrode in terms of the electrochemical activity for hydrazine oxidation using cyclic voltammetry (CV). Additionally, the temperature dependence and the mechanism of hydrazine oxidation reaction on Au/TiO_2-NTs have been discussed. The surface morphology and element analysis of gold coating on titanium dioxide nanotubes were characterized by scanning electron microscopy (SEM) and energy-dispersive X-ray spectroscopy (EDX), respectively.

2. Experimental

2.1. Chemicals, solutions and electrochemical equipment

Hydrazine (Merck) and dimethyl sulfoxide (DMSO) (Merck) were used as received. All other chemicals were of analytical grade and used without further purification. All electrochemical experiments were carried out at room temperature. Distilled water was used throughout. The electrochemical experiments were performed in a three-electrode cell assembly. A platinum sheet of the geometric area of about 20 cm^2 was used as counter electrode, while all potentials were measured with respect to a commercial saturated calomel electrode (SCE). Electrochemical experiments were carried out using a Princeton Applied Research, EG&G PARSTAT 2263 Advanced Electrochemical System run by Powersuite Software.

2.2. Preparation of titanium dioxide nanotubes (TiO_2-NTs) catalyst support

TiO_2-NTs arrays were prepared by anodizing of pure titanium sheet in a non-aqueous fluoride-containing electrolyte. Titanium discs were cut from a titanium sheet (purity %99.99, 1 mm thickness) and mounted using polyester resin. Titanium samples were degreased by sonicating in acetone and ethanol followed by rinsing with distilled water. Anodic films were grown from titanium by potentiostatic anodizing in a DMSO electrolyte containing 2 vol.% HF at a constant voltage of 40 V for 8 h at room temperature using a platinum sheet as counter electrode.

2.3. Preparation of Au/TiO_2-NTs/Ti catalysts

Au/TiO_2-NTs/Ti catalysts were prepared by the electrodeposition of gold on as-prepared TiO_2-NTs/Ti support. Electrodeposition experiments were carried out at a water-bath thermostat. After anodizing of titanium, the samples were ultrasonically cleaned in distilled water for 10–20 min to remove surface contaminants. Then the TiO_2-NTs/Ti electrodes were immerged into the bath for electrolytic deposition. Deposition of gold on TiO_2-NTs/Ti electrodes was performed under galvanostatic conditions. The deposition conditions were a current density of 5 mA/cm^2 for 10 min, in an acid bath containing $KAu(CN)_2$ in presence of a pH 4 citrate buffer. The temperature is maintained at 45 °C.

2.4. Physical characterization

Morphology, alignment, and composition of the TiO_2 nanotubes array and gold coating on TiO_2-NTs/Ti substrates were characterized with a Philips scanning electron microscope (SEM) and EDX.

3. Results and discussion

3.1. Characterization of the electrodes morphology

Fig. 1 shows SEM micrographs of the titanium dioxide nanotubes prepared by anodic oxidation. The average tube diameter

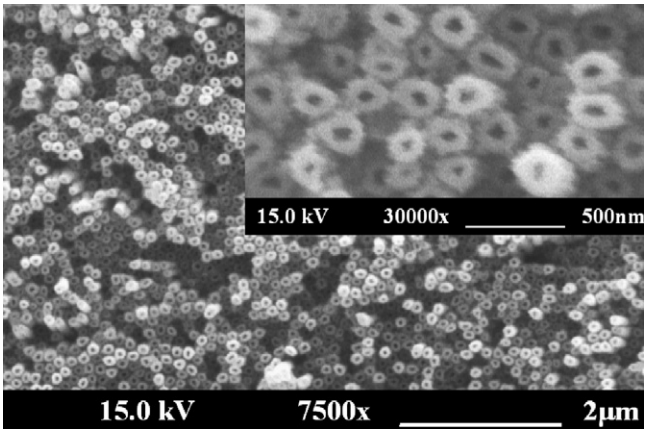

Fig. 1. The surface morphology of the TiO_2-NTs/Ti as support prepared by anodizing of titanium.

was about 50–80 nm, which can be used as good carrier of particle catalyst. Also the thickness of TiO_2-NTs layer was in the range of 100–140 nm. Fig. 2 illustrates the SEM micrographs of gold nanoparticles electrodeposited on titanium dioxide nanotubes. It can be seen that the gold nanoparticles with diameters around 30–40 nm are distributed in an almost homogeneous manner on top of TiO_2 nanotubes. Fig. 3 shows the EDX spectrum of Au/TiO_2-NTs/Ti after 10 min electroplating of gold on anodized titanium.

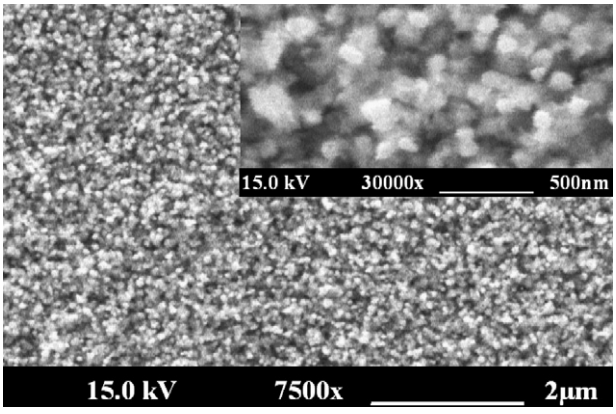

Fig. 2. The surface morphology of gold coating on the Au/TiO_2-NTs/Ti electrode.

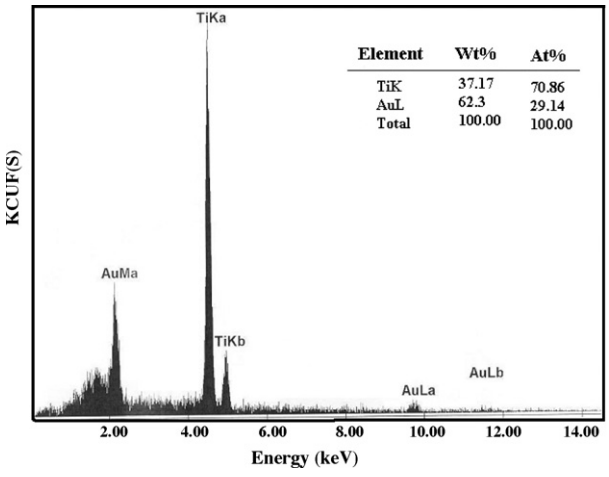

Fig. 3. EDX of Au/TiO_2-NTs/Ti electrode after 10 min electroplating of gold on anodized titanium.

EDX results confirm the presence of gold nanoparticle in the surface film.

3.2. Characterization of the Au/TiO_2-NTs/Ti catalysts surface

To ensure good electrical contact between the gold and underlying titanium electrode, the Au/TiO_2-NTs/Ti samples were tested as electrodes using a one electron redox couple. Fig. 4 shows the voltammetric curves for the reduction of $K_3[Fe(CN)_6]$ on Au/TiO_2-NTs/Ti and flat gold electrodes. The voltammogram for the Au/TiO_2-NTs/Ti electrode shows the expected reversible behavior for the reduction on a flat gold electrode. It suggests that the adhesion and electrical contact of the electrodeposited gold film with titanium is quite satisfactory.

3.3. Determination of catalysts surface area

In order to compare prepared electrodes with pure gold electrode and to electrochemically characterize the real surface of the Au/TiO_2-NTs/Ti electrode, the surface area of the electrode was determined using 1 mM $K_4Fe(CN)_6$ in 0.1 M KNO_3 by recording the cyclic voltammograms. From the cyclic voltammetric peak current and the diffusion coefficient of hexacyanoferrate, the surface area of the electrode was calculated by using the Eq. (1) [25,26]:

$$i_{pa} = (2.69 \times 10^5) n^{3/2} A D_o^{1/2} \nu^{1/2} C_o^* \quad (1)$$

where n is the number of electrons transferred, i.e. 1, A the surface area of the electrode, D_o the diffusion coefficient (9.382×10^{-6} cm^2 s^{-1}), ν the scan rate (100 mV s^{-1}), and C_o^* the concentration of electro-active species (1 mM). The surface area of Au/TiO_2-NTs/Ti electrode was found to be 6.75 cm^2 while the flat gold electrode gives a much smaller real surface area of 0.66 cm^2. The surface area of Au/TiO_2-NTs/Ti electrode was estimated to be about 10 times of flat gold electrode. Also, other confirmation experiment was performed, i.e. cyclic voltammetry of Au/TiO_2-NTs/Ti electrode in a 0.5 M H_2SO_4 solution was conducted (Fig. 5). It shows that the oxidation and reduction peak areas of Au/TiO_2-NTs/Ti electrode are much larger than the flat gold electrode. The real surface of the Au/TiO_2-NTs/Ti electrode is 6.8 cm^2, while the flat gold electrode gives a much smaller real surface area of 0.67 cm^2.

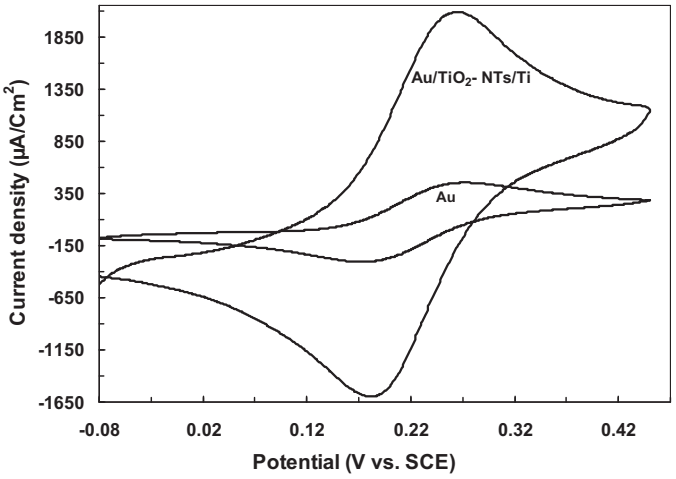

Fig. 4. Cyclic voltammograms for a Au/TiO_2-NTs/Ti electrode and a flat gold electrode, recorded at 100 mV s^{-1} in a solution containing 10 mM $K_3[Fe(CN)_6]$ in 1 M KCl at 25 °C.

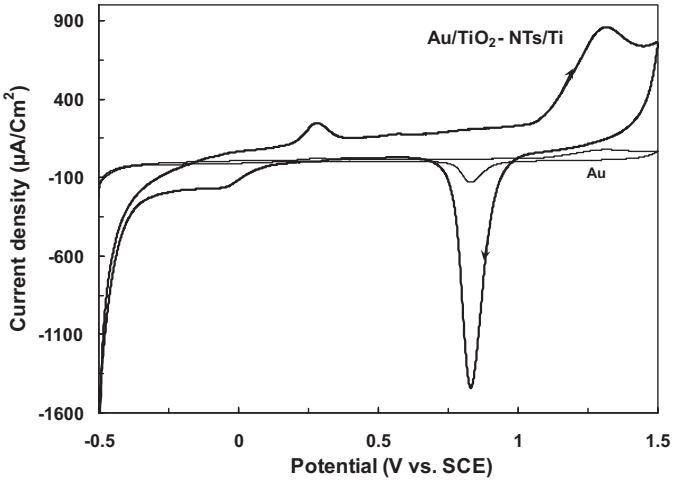

Fig. 5. Cyclic voltammograms for Au/TiO_2-NTs/Ti and flat gold electrodes in 0.5 M H_2SO_4 at 25 °C with a scan rate of 100 mV s^{-1}.

3.4. Cyclic voltammetric study of hydrazine electro-oxidation on the electrodes

In order to compare Au/TiO_2-NTs/Ti electrode with flat gold electrode, the cyclic voltammetry method was used to estimate the electro-catalytic behavior of the electrodes. Fig. 6 presents cyclic voltammograms of flat gold and Au/TiO_2-NTs/Ti electrodes in 0.1 M phosphate buffer–0.00085 M hydrazine aqueous solution, at a scan rate of 100 mV s^{-1}. The current density for hydrazine oxidation on Au/TiO_2-NTs/Ti electrode is greater than that observed for gold electrode. This result may also be attributed to the larger specific surface area of the Au/TiO_2-NTs/Ti electrodes. In addition to clarify if the increase of the specific area is the only factor to explain the increase of the oxidation current or the modification of the electrode provides new reaction pathways, decreasing the activation energy barrier of the reaction; the temperature dependency of hydrazine oxidation on Au/TiO_2-NTs/Ti and flat gold electrodes were investigated in the temperature range of 310–335 K by cyclic voltammetry and it was seen that anodic current increased as the temperature increased. Arrhenius plots for the anodic current of

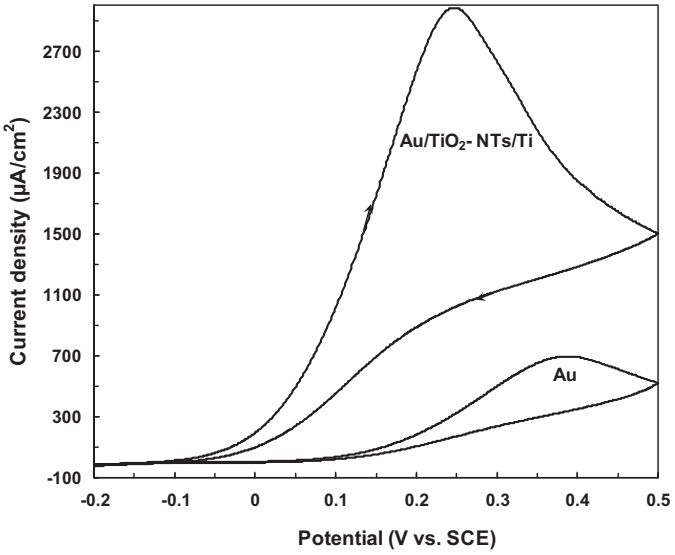

Fig. 6. Cyclic voltammograms for Au/TiO_2-NTs/Ti and flat gold electrodes in 0.1 M phosphate buffer–0.00085 M hydrazine aqueous solution at 25 °C with a scan rate of 100 mV s^{-1}.

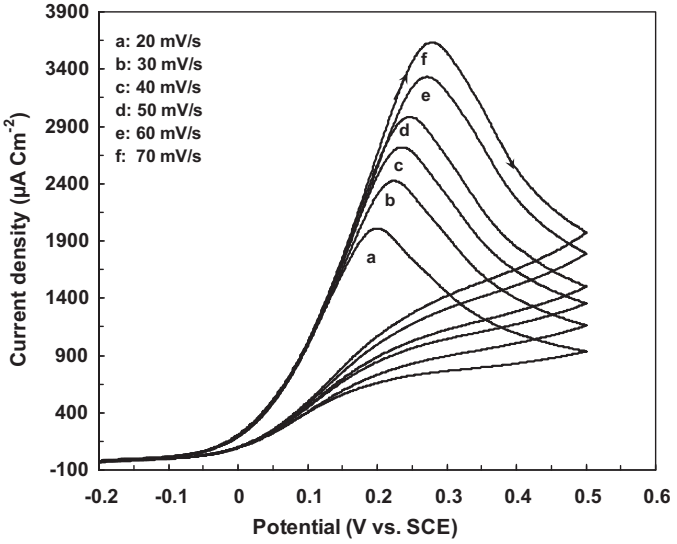

Fig. 7. The cyclic voltammograms of hydrazine on Au/TiO_2-NTs/Ti electrode at different scan rate.

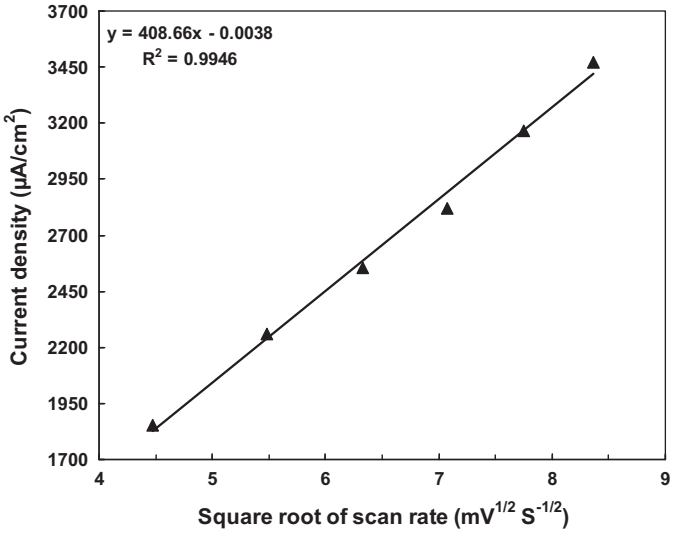

Fig. 8. The plot of hydrazine oxidation peak current on the Au/TiO_2-NTs/Ti electrode versus $\nu^{1/2}$.

hydrazine oxidation on Au/TiO_2-NTs/Ti and flat gold electrodes showed a linear correlation by plotting $\ln i$ versus $1/T$. The apparent activation energy for Au/TiO_2-NTs/Ti electrode was found to be lower than Au electrode. Thus increasing of the specific area and decreasing of activation energy are two parameters leading to increase in the oxidation current.

3.5. Effect of scan rate

The effect of different scan rates on the electro-catalytic properties of Au/TiO_2-NTs/Ti electrode toward hydrazine oxidation has been studied and results were shown in Fig. 7. As can be seen from Fig. 7, the increase in potential scan rate induced an increase in the electro-catalytic peak current and resulted in a shift to more positive potential value for the catalytic oxidation of hydrazine. This clear shift of the peak potential was occurred as expected for irreversible electrochemical reactions [27]. The obtained cyclic voltammograms were used to examine the variation of oxidation peak current versus scan rate. The oxidation current of hydrazine increased linearly with the square root of scan rate on Au/TiO_2-NTs/Ti electrode (Fig. 8), suggesting that the reaction is mass transfer controlled. In order to get the information on the rate determining step, Tafel slope, b, was determined using the following equation valid for a totally irreversible diffusion controlled process [28]:

$$E_p = 0.5b \log \nu + \text{constant} \quad (2)$$

Therefore, on the basis of Eq. (2), the slope of E_p versus $\log \nu$ plot is:

$$\frac{dE_p}{d \log \nu} = \frac{b}{2} \quad (3)$$

where b is the Tafel slope and ν is the scan rate; the Tafel slope can also be expressed as:

$$b = 2.3RT(\alpha_a n_\alpha F)^{-1} \quad (4)$$

On the basis of these equations, the slope of the plots of E_p versus $\log \nu$ is $b/2$ which was found equal to 0.137 in this work (Fig. 9), so, $b = 0.274$ V. Assuming one electron transfer in the rate-determining step ($n_\alpha = 1$), these slope values indicate a transfer coefficient (α) equal to 0.21.

The number of electrons (n) involved in the overall reaction can also be obtained from the slope of I_p versus $\nu^{1/2}$ according to the following equation [29].

$$I_p = 3.01 \times 10^5 n[(1-\alpha)n\alpha]^{1/2} A C_s D^{1/2} \nu^{1/2} \quad (5)$$

where A is electrode surface area, C_s is hydrazine concentration and D is diffusion coefficient. Considering $D = 4.1 \times 10^{-5}$ cm^2 s^{-1} (diffusion coefficient was calculated from chronoamperometry), from the slope of I_p versus $\nu^{1/2}$ plot, the total number of electrons (n) involved in the oxidation is evaluated to be 4.

The mechanism of hydrazine oxidation depends significantly on the electrolyte solution and the nature of the electrodes. According to Xie et al., under solution conditions, hydrazine was mainly present in its unprotonated form, and the protonated form which presented only a small extent, therefore, following mechanism could be proposed for the oxidation of hydrazine at the Au/TiO_2-NTs/Ti electrode [30].

$$N_2H_4 + H_2O \rightarrow N_2H_3 + H_3O^+ + e^- \quad \text{(slow)} \quad \text{(I)} \quad (6)$$

$$N_2H_3 + 3H_2O \rightarrow N_2 + 3H_3O^+ + 3e^- \quad \text{(fast)} \quad \text{(II)} \quad (7)$$

The rate-determining step is one electron transfer followed by a 3-electron process to give N_2 as a final product. The overall reaction

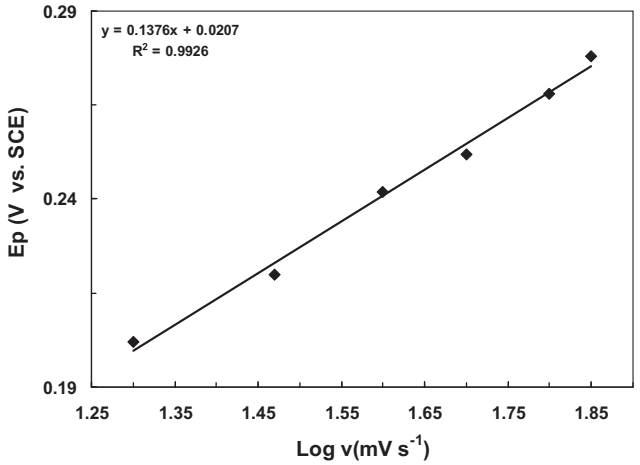

Fig. 9. The peak potential dependence on log ν for the oxidation of hydrazine at the Au/TiO_2-NTs electrode.

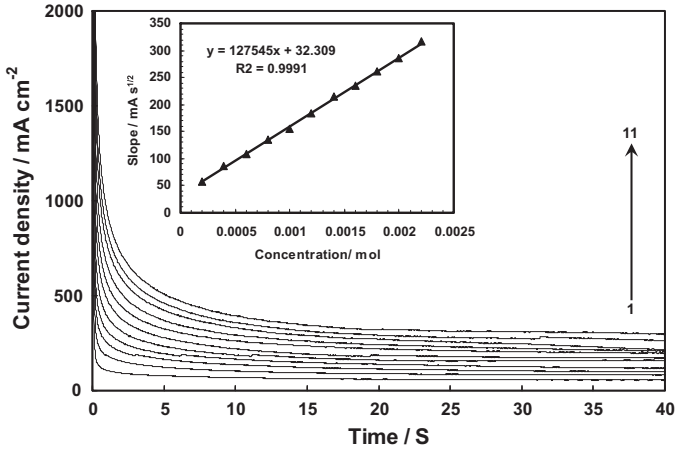

Fig. 10. Chronoamperometric response of Au/TiO_2-NTs/Ti electrode in 0.1 M phosphate buffer solution containing different concentrations of hydrazine. The numbers 1–11 correspond to 0.2–22 mM hydrazine, respectively. Insets: Variation of chronoamperometric currents at $t = 20$ s vs. concentration of hydrazine.

of hydrazine oxidation can be expressed as following reaction:

$$N_2H_4 + 4H_2O \rightarrow N_2 + 4H_3O^+ + 4e^- \quad (8)$$

Chronoamperometry was used for measurement of the diffusion coefficient of hydrazine by setting the Au/TiO_2-NTs/Ti electrode potential at 400 mV for various concentrations of hydrazine. For hydrazine with diffusion coefficient of D, the current of the electrochemical reaction (at a mass transport limited rate) is described by the Cottrell equation [31]:

$$I = nFAD^{1/2}C_s\pi^{-1/2}t^{-1/2} \quad (9)$$

Based on the Cottrell equation, the plot of I versus $t^{-1/2}$ be linear. We have carried out such studies for various hydrazine concentrations at the Au/TiO_2-NTs/Ti electrode. The slopes of the resulting lines were then plotted versus the concentration of hydrazine (inset of Fig. 10). From using the Cottrell equation, a diffusion coefficient was calculated 4.1×10^{-5} cm^2 s^{-1} (Fig. 11). This value of diffusion coefficient is in agreement with 1.15×10^{-5} cm^2 s^{-1} [32], 1.39×10^{-5} cm^2 s^{-1} [33] 4×10^{-5} cm^2 s^{-1} [34,35] that are reported in the literature.

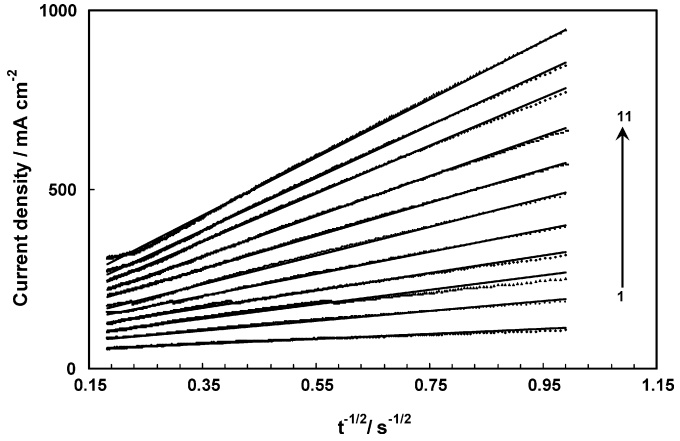

Fig. 11. Plot of I vs. $t^{-1/2}$ obtained from chronoamperometric experiments for a Au/TiO_2-NTs/Ti electrode in 0.1 M phosphate buffer solution (pH 7.0) containing different concentrations of hydrazine.

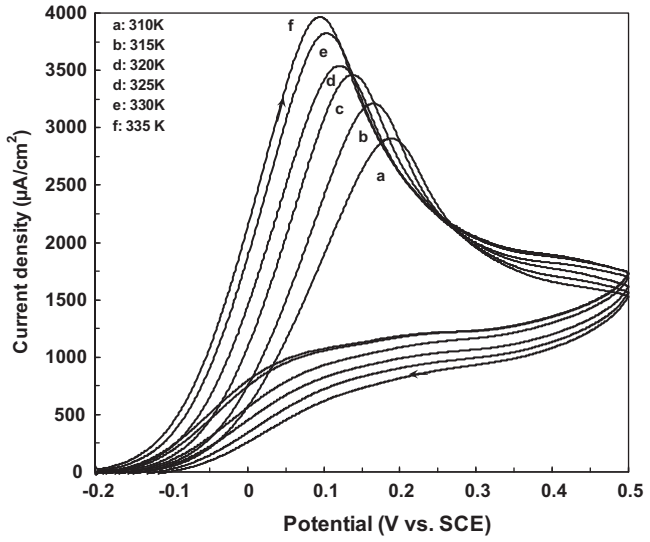

Fig. 12. The effect of temperature on cyclic voltammograms of hydrazine oxidation on Au/TiO_2-NTs/Ti electrode in the range of 310–335 K.

3.6. The temperature dependence of hydrazine oxidation on Au/TiO_2-NTs/Ti electrode

Temperature is one of the most important factors affecting the reaction rate. In order to study electro-catalytic performance of Au/TiO_2-NTs/Ti electrodes on the electrolyte temperature, the temperature dependency of hydrazine oxidation on Au/TiO_2-NTs/Ti electrode was investigated in the temperature range of 310–335 K by the method of cyclic voltammetry. From Fig. 12, it can be seen that anodic current increase with temperature. Also as can be seen from Fig. 12, increase in temperature leads to a shift of anodic peak toward more negative potentials due to the more feasibility of oxidation at elevated temperatures. Fig. 13 presents the relationship between the experimental temperature and the hydrazine electro-oxidation current density. As the temperature increases, the electro-oxidation current density increases. This is attributed to the increase in the rate of charge transfer at electrode/electrolyte interface. At the same time, high temperature will decrease the increases diffusion phenomena, so higher electro-oxidation currents could be obtained.

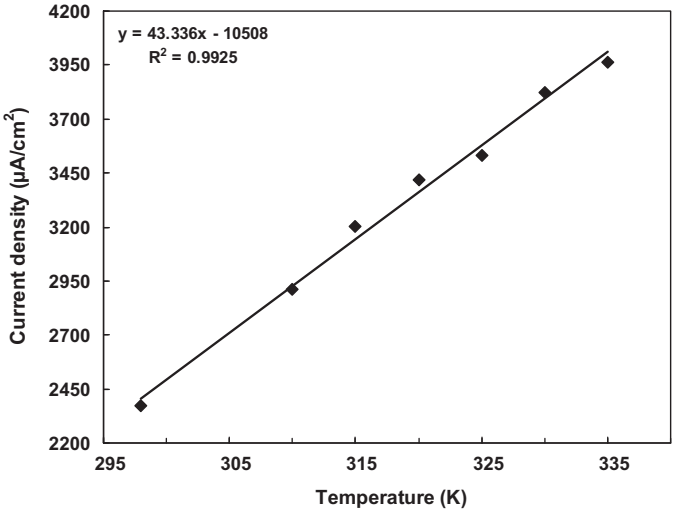

Fig. 13. Relationship between electro-oxidation current density and temperature. Electrolyte 0.1 M phosphate buffer–0.00085 M hydrazine aqueous solution.

4. Conclusions

Au/TiO_2-NTs/Ti electrode was prepared by a two-step process consisting of anodic oxidation of titanium followed by cathodic electrodeposition of gold on TiO_2 nanotubes. The morphology and electro-catalytic performance of the electrode was investigated by scanning electron microscopy and cyclic voltammetry, respectively. The results indicated that gold nanoparticles were homogeneously deposited on the surface of TiO_2 nanotubes. These electrodes presented a good electro-catalytic activity toward the oxidation of hydrazine. The electro-catalytic activity of the Au/TiO_2-NTs/Ti electrodes and flat gold toward hydrazine oxidation was evaluated by electrochemical voltammograms. Results showed that the flat gold electrode could not be considered suitable for oxidation of hydrazine. However, the Au/TiO_2-NTs/Ti electrode was shown to possess high catalytic activity toward the oxidation reaction of hydrazine. The oxidation kinetic of hydrazine is also studied. The results indicated that the oxidation process is diffusion controlled. Finally temperature dependence of hydrazine oxidation on Au/TiO_2-NTs/Ti electrode was investigated.

Acknowledgment

The authors would like to acknowledge the financial support of the Office of Vice Chancellor in Charge of Research of University of Tabriz.

References

[1] X. Ren, M.S. Wilson, S. Gottesfeld, J. Electrochem. Soc. 143 (1996) L12.
[2] C. Lamy, J.M. Leger, Proceedings of the First International Symposium on New Material Fuel Cell Systems, vol. 296, 1995.
[3] W.X. Yin, Z.P. Li, J.K. Zhu, H.Y. Qin, J. Power Sources 182 (2008) 520–523.
[4] A.J. Bard, Anal. Chem. 35 (1963) 1602–1607.
[5] K. Yamada, K. Yasuda, N. Fujiwara, Z. Siroma, H. Tanaka, Y. Miyazaki, T. Kobayashi, Electrochem. Commun. 5 (2003) 892–896.
[6] K. Asazawa, K. Yamada, H. Tanaka, A. Oka, M. Taniguchi, T. Kobayashi, Angew. Chem. Int. Ed. 46 (2007) 8024–8027.
[7] K. Yamada, K. Yasuda, H. Tanaka, Y. Miyazaki, T. Kobayashi, J. Power Sources 122 (2003) 132–137.
[8] B.B. Dong, L. He, J. Huang, G.Y. Gao, Z. Yang, H.L. Li, J. Power Sources 175 (2008) 266–271.
[9] M.D. García Azorero, M.L. Marcos, J. González Velasco, Electrochim. Acta 39 (1994) 1909–1914.
[10] F. Li, B. Zhang, E. Wang, S. Dong, J. Electroanal. Chem. 422 (1997) 27–33.
[11] D. Guo, H. Li, J. Colloid Interface Sci. 286 (2005) 274–279.
[12] D. Guo, H. Li, Electrochem. Commun. 6 (2004) 999–1003.
[13] G. Gao, D. Guo, H. Li, Electrochem. Commun. 9 (2007) 1582–1586.
[14] K.I. Ozoemena, T. Nyokong, Talanta 67 (2005) 162–168.
[15] J. Li, X. Lin, Sens. Actuators, B 126 (2007) 527–535.
[16] R. Ganesan, J.S. Lee, J. Power Sources 157 (2006) 217–221.
[17] J. Wang, M. Musameh, Y. Lin, J. Am. Chem. Soc. 125 (2003) 2408–2409.
[18] B.B. Dong, L. He, Y.M. Chai, C.G. Liu, Mater. Chem. Phys. 120 (2010) 404–408.
[19] M.G. Hosseini, S.A.S. Sajjadi, M.M. Momeni, Surf. Eng. 23 (2007) 419–424.
[20] M.G. Hosseini, M.M. Momeni, M. Faraji, J. Appl. Electrochem. 40 (2010) 1421–1427.
[21] M.G. Hosseini, S.A.S. Sajjadi, M.M. Momeni, IUST Int. J. Eng. Sci. 7 (2008) 39–42.
[22] M.G. Hosseini, M.M. Momeni, J. Solid State Electrochem. 14 (2010) 1109–1115.
[23] M.G. Hosseini, M.M. Momeni, J. Mater. Sci. 45 (2010) 3304–3310.
[24] M.G. Hosseini, M.M. Momeni, M. Faraji, J. Mater. Sci. 45 (2010) 2365–2371.
[25] A.J. Bard, L.R. Faulkner, Electrochemical Methods Fundamentals and Applications, 2nd edn, Wiley, New York, 2004.
[26] D.K. Gosser, Cyclic Voltammetry, VCH, New York, 1994.
[27] C. de la Fuente, J.A. Acuna, M.D. Vasquez, M.L. Tascon, M.I. Gomez, P.S. Batanero, Talanta 44 (1997) 685–695.
[28] M.H. Pournaghi-Azar, H. Razmi-Nerbin, J. Electroanal. Chem. 488 (2000) 17–24.
[29] S. Antoniadou, A.D. Jannakoudakis, E. Theodoridou, Synth. Met. 30 (1980) 295–304.
[30] J. Li, H. Xie, L. Chen, Sens. Actuators, B – Chem. doi:10.1016/j.snb.2010.10.040.
[31] C.P. Andrieux, J.M. Saveant, J. Electroanal. Chem. 93 (1978) 163–168.
[32] S.M. Golabi, H.R. Zare, M. Hamzehloo, Microchem. J. 69 (2001) 111–121.
[33] J. Zheng, Q. Sheng, L. Li, Y. Shen, J. Electroanal. Chem. 611 (2007) 155–161.
[34] L. Niu, T. You, J.Y. Gui, E. Wang, S. Dong, J. Electroanal. Chem. 448 (1998) 79–86.
[35] B. Wang, X. Cao, J. Electroanal. Chem. 309 (1991) 147–158.